Journal of Biomolecular NMR (2005) 32: 263–271
DOI 10.1007/s10858-005-8872-1

Article

Resolution-enhanced base-type-edited HCN experiment for RNA

Hélène Van Melckebeke[a], Arthur Pardi[b], Jérôme Boisbouvier[a], Jean-Pierre Simorre[a] & Bernhard Brutscher[a,*]

[a]*Laboratoire de RMN, Institut de Biologie Structurale - Jean-Pierre Ebel, UMR, 5075 CNRS-CEA-UJF, 41, rue Jules Horowitz, 38027, Grenoble Cedex, France;* [b]*Department of Chemistry and Biochemistry, UCB 215, Boulder, CO, 80309-0215, USA*

Received 28 January 2005; Accepted 7 June 2005

Key words: base-type selection, HCN, NMR, resonance assignment, RNA, spectral editing

Abstract

New base-type-edited transverse-relaxation optimized CT-HCN(C) experiments are presented that yield intra-base and sugar-to-base correlations for $^{13}C-^{15}N$ labeled RNA. High spectral resolution in the ^{13}C and ^{15}N dimensions is achieved by constant time (CT) frequency editing. A spectral editing filter applied during the CT ^{15}N labeling period separates the correlation peaks arising from G/U and A/C nucleotide bases. This provides the increased spectral resolution required to unambiguously connect the ^{1}H and ^{13}C resonances in sugar and base moieties of RNA nucleotides. In addition, the experiment allows base type identification for each residue, and therefore presents an attractive spectroscopic alternative to nucleotide-specific isotope labeling. Application to a 33-nucleotide RNA aptamer demonstrates the performance of the new pulse scheme.

Introduction

HCN-type correlation experiments (Sklenar et al., 1993a; Farmer et al., 1994) are important for resonance assignment of nucleic acids (Wijmenga and van Buuren, 1998; Furtig et al., 2003). They provide intranucleotide sugar-base connectivity information by correlating the base C_6, H_6 (pyrimidines) or C_8, H_8 (purines) with the sugar $C_{1'}$, and $H_{1'}$, nuclei. Recently, HCN experiments have also shown to be useful for the measurement of scalar and residual dipolar spin–spin couplings in RNA (Yan et al., 2002; Jaroniec et al., 2005), or of cross-correlated relaxation rates related to the torsion angle χ_1 (Ravindranathan et al., 2003; Duchardt et al., 2004) to obtain complementary structural information to NOE-derived distance restraints. Different implementations of the HCN sugar-to-base correlation experiment have been proposed in the past. In the most common approach, two separate correlation peaks are detected for the sugar and the base moieties. The two peaks corresponding to the same nucleotide are then identified via the shared ^{15}N chemical shift of the nitrogen in the glycosidic bond, N_1 in pyrimidines and N_9 in purines (Figure 2a). To increase the intrinsically low sensitivity of the out-and-back HCN experiment (due to the small $^{1}J_{CN} \approx 12$ Hz scalar coupling constant), transverse-relaxation optimized pulse sequences have been proposed exploiting either the favorable relaxation properties of multiple-quantum coherence (Marino et al., 1997; Fiala et al., 1998), or the interference of the ^{13}C CSA and $^{1}H-^{13}C$ dipolar relaxation mechanisms, also known as the TROSY effect (Fiala et al., 2000; Riek et al., 2001), or a combination of both (Brutscher and Simorre, 2001).

*To whom correspondence should be addressed: E-mail: Bernhard.Brutscher@ibs.fr

For application to larger RNA, however, increased ^{15}N chemical shift overlap makes unambiguous peak assignment difficult. To overcome this problem, unidirectional HCNCH experiments have been proposed (Farmer et al., 1993; Sklenar et al., 1993b; Tate et al., 1994; Hu et al., 2001) which correlate directly the sugar ^{1}H and ^{13}C with those of the base. Unfortunately, these experiments are even less sensitive than the out-and-back HCN experiment due to the additional transfer steps. An HC(N)C-type out-and-back correlation experiment has also been proposed recently (Furtig et al., 2004). In this pulse scheme magnetization is further transferred from $N_{1/9}$ to the quaternary C_2 or C_4 base carbons, which are frequency labeled to provide the required frequency match between sugar and base correlations. Other alternatives to increase spectral resolution include the preparation of different nucleotide-specific isotope-labeled RNA samples. This solution offers the advantage of reduced spectral overlap and provides additional base type information, but the production of four selectively isotope-labeled RNA samples is costly and labor intensive. In addition, NMR data have to be acquired for each of the 4 samples. Here we present new 3D transverse-relaxation optimized CT-HCN(C) experiments for uniformly ^{13}C, ^{15}N labeled RNA. CT frequency editing provides high spectral resolution in both, the ^{13}C and ^{15}N frequency dimensions. A base-type editing filter further increases spectral resolution and facilitates the assignment of sugar and base HCN correlation peak pairs. The experiment also allows base-type identification without the need of selective isotope labeling. The performance of the new pulse sequence is demonstrated for a 33-nucleotide RNA aptamer in complex with theophylline.

Materials and methods

Sample preparation

The uniformly ^{13}C, ^{15}N-labeled 33-nucleotide RNA aptamer – theophylline complex was prepared as described elsewhere (Zimmermann et al., 1997). Two samples were used for this study containing a 1: 1.2 RNA complex with theophylline at concentrations of about 1.0 and 0.7 mM dissolved in a D_2O solution at pH 6.8 containing 20 mM sodium phosphate, 30 mM NaCl, and 2 mM $MgCl_2$.

NMR data acquisition and processing

NMR experiments were performed on a Varian INOVA 800 spectrometer, equipped with a triple-resonance (^{1}H, ^{13}C, ^{15}N) probe and shielded z-axis gradients. The sample temperature was set to 25 °C. For the 2D CT-H(C)N(C) spectrum shown in (Figure 4), the time variable t_2 was set to $t_2 = 0$. A data set of 2-times (base-type editing filter) 180 (^{15}N) × 512 (^{1}H) complex points were recorded in an overall experimental time of 14 h. The spectral widths were set to 3600 Hz (^{15}N), and 10000 Hz (^{1}H). Additional 2D CT-HC(NC) spectra recorded using either the sensitivity enhanced TROSY (Figure 1a) or the MQ-TROSY version (Figure 1b) of the experiment were recorded with 78 (^{13}C) × 512 (^{1}H) complex points for spectral widths of 5000 Hz (^{13}C), and 10000 Hz (^{1}H) in an experimental time of 1.5 h. No base-type selection was performed, as the aim of this experiment was to compare the relative sensitivity of the two implementations of the CT-HCN(C) experiment. Data processing was performed using the FELIX program version 2000 (Accelrys Inc.). Mirror image linear prediction was applied (Zhu and Bax, 1990) to double the acquisition times of the ^{15}N CT dimension prior to squared cosine apodization, zero-filling and Fourier transformation.

Results and discussion

Figure 1 shows two implementations of the new CT-HCN(C) experiment developed to record high-resolution HCN correlation spectra for resonance assignment of RNA. The flow of magnetization is given as follows:

$$\begin{aligned} H_{6/8/1'} \xrightarrow{J_{CH}} C_{6/8/1'} \xrightarrow{J_{CN}} N_{1/9}[CT - t_1, base - type\ filter] \\ \xrightarrow{J_{CN}} C_{6/8/1'}[CT - t_2] \xrightarrow{J_{CH}} H_{6/8/1'}[t_3] \end{aligned} \quad (1)$$

with the active spin–spin couplings indicated above the arrows. Both pulse sequences are of the out-and-back type with the standard coherence transfer pathway of HCN experiments. In (a) TROSY-type (Pervushin et al., 1997) ^{13}C evolution is implemented for both the base and sugar moieties during the $^{13}C \rightarrow {}^{15}N$ transfer steps,

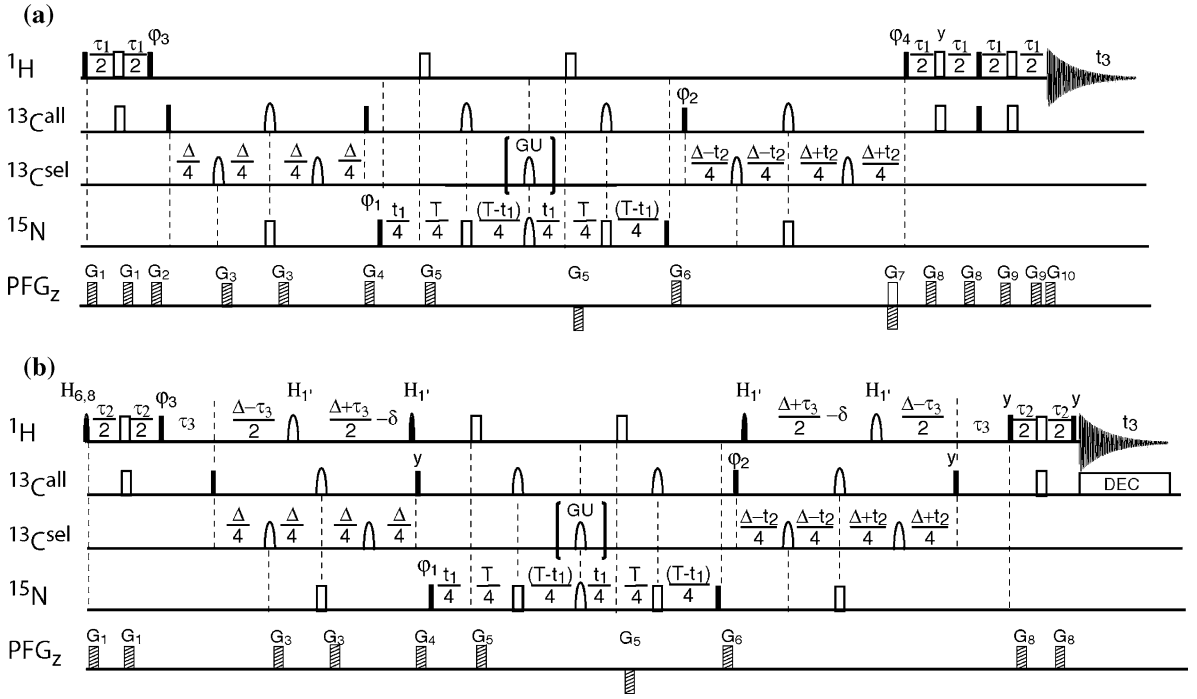

Figure 1. Pulse sequences for base-type-edited (a) TROSY-CT-HCN(C) and (b) MQ-TROSY-CT-HCN(C) experiments of RNA. Two data sets are recorded with and without the GU-labeled pulse in brackets labeled (GU) on the $^{13}C^{sel}$ channel to perform base-type editing. The carrier frequencies are set to 4.7 ppm (^{1}H), 112 ppm ($^{13}C^{all}$), and 153 ppm (^{15}N) throughout the experiment. The pulses applied on the $^{13}C^{sel}$ channel, and the band-selective ^{1}H pulses (denoted $H_{6,8}$ and $H_{1'}$) in (b) are frequency shifted by time-proportional phase incrementation to the center of the desired frequency bands. All radio-frequency (rf) pulses are applied along the *x*-axis unless indicated. The phases φ_1 and φ_2 are initially set to $\varphi_1 = \varphi_2 = x$. The phase φ_3 is adjusted to *y* or $-y$ depending on the spectrometer (see text). 90° and 180° rf pulses are represented by filled and open pulse symbols, respectively. Shaped pulse symbols indicate band-selective or composite pulses: the shaped $^{13}C^{all}$ pulses are applied as symmetric composite refocusing pulses of the form $58_x - 140_{-x} - 344_x - 140_{-x} - 58_x$ (Shaka and Pines, 1987) adjusted to cover a band width of 120 ppm. Selective inversion pulses on the $^{13}C^{sel}$ channel applied during the transfer delays δ_2 have an IBURP-2 shape (Geen and Freeman, 1991) and are centered at 72 ppm ($C_{2'}$) and 160 ppm (C^{arom}), both covering a band width of 16 ppm. These two pulse shapes are combined to a single shape by vector addition (Kupce and Freeman, 1993). The $^{13}C^{sel}$ inversion pulse labeled (GU) required for base-type filtering is applied with an i-SNOB-5 shape (Kupce et al., 1995) covering a bandwidth of 5 ppm centered at 153.4 ppm. The selective ^{15}N pulse is applied with an r-SNOB profile (Kupce et al., 1995) centered at 155 ppm and covering a band width of 40 ppm. The $H_{6,8}$ excitation pulse is applied with an e-SNOB profile centered at 7.7 ppm and covering a bandwith of 2.0 ppm. The $H_{1'}$ refocusing and flipback pulses are applied with r-SNOB, and time- and phase-inverted e-SNOB pulse shapes, respectively, centered at 5.6 ppm and covering a bandwith of 1.4 ppm. The transfer delays were set to $\tau_1 = 2.65$ ms, $\tau_2 = 2.5$ ms, $\tau_3 = 2.8$ ms, $\Delta = 30$ ms, and $T = 57$ ms (including pulse lengths of ^{13}C pulses). The delay δ is set to the difference in pulse length between the composite 180° and the 90° $^{13}C^{all}$ pulses, and ensures complete refocusing of $H_{1'}$ transverse coherence. ^{13}C composite decoupling during acquisition is achieved using adiabatic WURST-2 decoupling (Kupce and Freeman, 1996) covering a band width of 120 ppm. Pulsed field gradients G_1–G_{10} are applied along the *z*-axis (PFG_z) with gradient strengths ranging from 10 to 20G/cm and lengths from 100 to 500 μs, followed by a recovery delay of 100μs. The relative strengths of the gradients G_7 and G_{10} have to be adjusted to the gyromagnetic ratios of ^{1}H and ^{13}C as $G_7/G_{10} = \gamma_H/\gamma_C$. A simple 2-step phase cycle is used with $\varphi_2 = x$, $-x$, and $\varphi_{rec} = x$, $-x$. Quadrature detection in t_1 (^{15}N) is obtained by incrementing the phase δ_1 according to STATES-TPPI. In (a) sensitivity-enhanced echo/antiecho quadrature detection in t_2 (^{13}C) is obtained by recording two data sets with the following phase settings: (I) $\varphi_2 = x$, $\varphi_4 = -y$, and (II) $\varphi_2 = y$, $\varphi_4 = y$. In addition the sign of G_7 is changed from minus to plus for the second data set. In (b) quadrature detection in t_2 (^{13}C) is obtained by incrementing the phase φ_2 according to STATES. Pulse sequences in Varian pulse sequence language and transformation protocols in Felix macro language can be obtained from the authors upon request.

whereas the pulse sequence shown in (b) is of the MQ-TROSY type (Brutscher and Simorre, 2001) using $^{1}H-^{13}C$ MQ coherence evolution for the sugar moieties and TROSY-type spin evolution for the base moieties.

In short, the coherence transfer pathway of the TROSY CT-HCN(C) experiment of Figure 1a is given as follows: the excited ^{1}H coherence H_y is transferred to the attached carbon via the $^{1}J_{CH}$ coupling yielding an anti-phase coherence $2H_zC_x$.

The same INEPT sequence also transfers the ^{13}C steady state magnetization C_z into an inphase coherence C_x. Both, inphase and anti-phase coherences are further transferred to the glycosidic nitrogen $N_{1,9}$. The transfer delay δ_2 is set to $2/J_{C6C5} \cong 30$ ms to refocus spin evolution due to the J_{C6C5} scalar coupling in pyrimidine residues. The band-selective inversion pulses applied on the $^{13}C^{sel}$ channel in Figure 1a remove the effects of other carbon–carbon couplings ($J_{C1'C2'}$, $J_{C8C6/4}$, J_{C6C2}). Then, the ^{15}N frequency is edited in a CT manner, with the CT delay T adjusted as explained below to allow the implementation of a base-type filter. ^{1}H and ^{13}C 180° pulses are used during T to refocus J_{NH} and J_{NC} coupling evolution. In addition the small homonuclear J_{N9N3} scalar coupling is refocused by a band-selective $N_{1,9}$ pulse applied at the centre of the CT delay. Finally, in the second half of the pulse sequence magnetization is transferred back to ^{1}H for final detection. Additional CT ^{13}C frequency editing is realized during the $^{15}N \rightarrow {}^{13}C$ back-transfer delay δ_2. No ^{1}H pulses are applied during the $^{13}C \rightarrow {}^{15}N$ transfer steps thus providing TROSY-type signal enhancement for both, the base and the sugar correlations. The double S^3CT transfer element (Pervushin et al., 1997; Sørensen et al., 1997), used for the $^{13}C \rightarrow {}^{1}H$ back-transfer, allows sensitivity-enhanced echo/antiecho quadrature detection in t_2 and selection of the slowly relaxing ^{13}C doublet line. As usual the phase ϕ_3 of the ^{1}H 90° pulse in the initial $^{1}H \rightarrow {}^{13}C$ INEPT transfer is spectrometer dependent and has to be adjusted ($\varphi_3 = y$ or $\varphi_3 = -y$) to add up the signals originating from the ^{1}H and ^{13}C steady-state magnetizations (Brutscher et al., 1998).

The major part of the MQ-TROSY CT-HCN(C) pulse sequence shown in (Figure 1b) is identical to the above-described TROSY version of (Figure 1a). The major modifications concern the $^{1}H \rightarrow {}^{13}C$ out and back-transfer steps. A specially designed pulse sequence element transforms ^{1}H spin polarization into $^{1}H-{}^{13}C$ MQ coherence for the sugar moieties, and into a single-transition state for the base moieties as described previously (Brutscher and Simorre, 2001). Additional band-selective $H_{1'}$ pulses are required to refocus ^{1}H chemical shift evolution during the transfer delays τ_3 and Δ, and to create antiphase single-quantum coherence $4N_y\,C_z\,H_z$ for ^{15}N CT frequency editing. A different zero-order phase correction along the ^{1}H dimension is required for the sugar and base moieties to account for the 90° phase shift between the $H_{1'}$ and $H_{6,8}$ coherences (Brutscher and Simorre, 2001) prior to detection. The MQ-TROSY version of the CT-HCN(C) experiment presents the additional advantage that the $^{1}H \rightarrow {}^{13}C$ transfer delays can be adjusted separately for the sugar (τ_3) and base (τ_2) ^{1}H—^{13}C spin pairs. However, it lacks the possibility of sensitivity-enhanced ^{13}C quadrature detection.

An experimental comparison of the two CT-HCN(C) experiments is shown in (Figure 2a–d) showing 2D $^{1}H-{}^{13}C$ spectra of the theophylline-apatamer RNA complex recorded at 800 MHz using the pulse sequences of (Figure 1a and 1b). The experiments were performed without base-type filtering, and setting the CT delay to $T = 2$ms, and $t_1 = 0$. The TROSY-only based version yields slightly higher peak intensity for the base moieties, whereas the MQ-TROSY implementation significantly enhances intensities of most cross peaks in the sugar region. However, for some cross peaks with $H_{1'}$ frequencies outside or et the edge of the frequency band covered by the $H_{1'}$ pulses the peak intensity is reduced with respect to the TROSY version, as illustrated for nucleotide U23 (Figures 2b and d).

The principal modifications of the new CT-HCN(C) with respect to existing implementations of the HCN experiment are the addition of a CT ^{15}N editing period and a base-type spectral editing filter. In general, CT frequency editing allows adjusting the spectral resolution $\Delta\nu_{res}$ by choosing a constant time delay $T = 1/\Delta\nu_{res}$, albeit at the expense of the overall sensitivity of the experiment. The relative sensitivity of the CT versus non-CT HCN experiment depends on the $N_{1/9}$ transverse relaxation rates which are dominated by the ^{15}N chemical shift anisotropy (CSA) contribution, and the desired spectral resolution in the ^{15}N dimension. Additional base-type spectral editing is realized during the CT delay T. The filter implemented in the pulse sequence of Figure 1 exploits different properties of the involved spin systems: (i) the presence of a scalar coupling between $N_{1,9}$ to a quaternary carbon C_4 (purines) or C_2 (pyrimidines) (see Figure 3a), with a coupling constant of $^{1}J_{N9C4} = {}^{1}J_{N1C2} \approx 20$ Hz for A, G, and U, and $^{1}J_{N1C2} \approx 12$ Hz for C nucleotides (Wijmenga and van Buuren, 1998), (ii) the fact that the quaternary C_4 and C_2 carbons resonate in distinct frequency ranges for the different nucleotides.

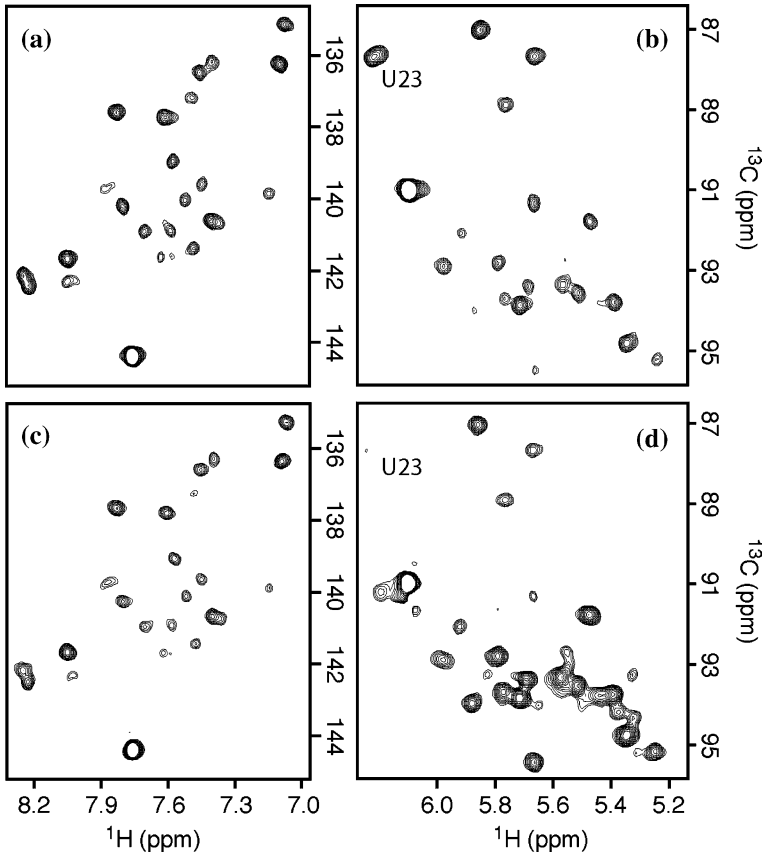

Figure 2. Comparison of 2D $^{1}H-^{13}C$ correlation spectra recorded (a) and (b) using the TROSY CT-HCN(C) sequence of Figure 1a, and (c) and (d) using the MQ-TROSY CT-HCN(C) sequence of Figure 1b without base-type spectral editing and setting $t_1 = 0$. Both spectra were recorded in the same experimental time of 1.5 h. The regions of the spectra corresponding to the H_8-C_8 and H_6-C_6 correlations are shown in (a) and (c), whereas the regions corresponding to the $H_{1'}$-$C_{1'}$ correlations are shown in (b) and (d).

As shown in (Figure 3b) 3 frequency bands can be distinguished, thus allowing for Hadamard-type spectral editing (Hadamard, 1893; Kupce and Freeman, 2003; Van Melckebeke et al., 2004). Because of their overlapping $C_{2,4}$ chemical shift ranges, a frequency-based spectral editing filter does not allow to discriminate between G and U nucleotides. We have designed a filter acting on only two bands corresponding to either G + U or A + C resonances. As will be seen later, this simple 2-step filter is sufficient to discriminate between all four nucleotide types. The filter requires the acquisition of only two data sets. In the first experiment, the pulse denoted GU on the $^{13}C^{sel}$ channel in Figure 1 is omitted, and no scalar $^{1}J_{N9C4}$ or $^{1}J_{N1C2}$ coupling evolution occurs during the CT delay T. In the second experiment, a selective inversion pulse is applied covering the $C_{2,4}$ band of G and U bases (see Figure 3b). This induces an additional $^{1}J_{N9C4}$ and $^{1}J_{N1C2}$ coupling evolution during the delay T for spin systems corresponding to U or G nucleotides, while spin evolution for C and A nucleotides is not changed by this pulse. If the delay T is adjusted to $T = 1/J_{N9C4}(G) = 1/J_{N1C2}(U)$, this results in a sign change of the observed NMR signal for U and G residues. Addition of the two experiments leads to a spectrum containing exclusively HCN correlation peaks from A and C, whereas subtraction provides the corresponding spectrum for G and U nucleotides. Note that the base-type-edited CT-HCN(C) experiment retains the full sensitivity of the CT-HCN experiment of the same duration, because no additional spin evolution period is required, and the full NMR signal is detected (sign-modulated) in

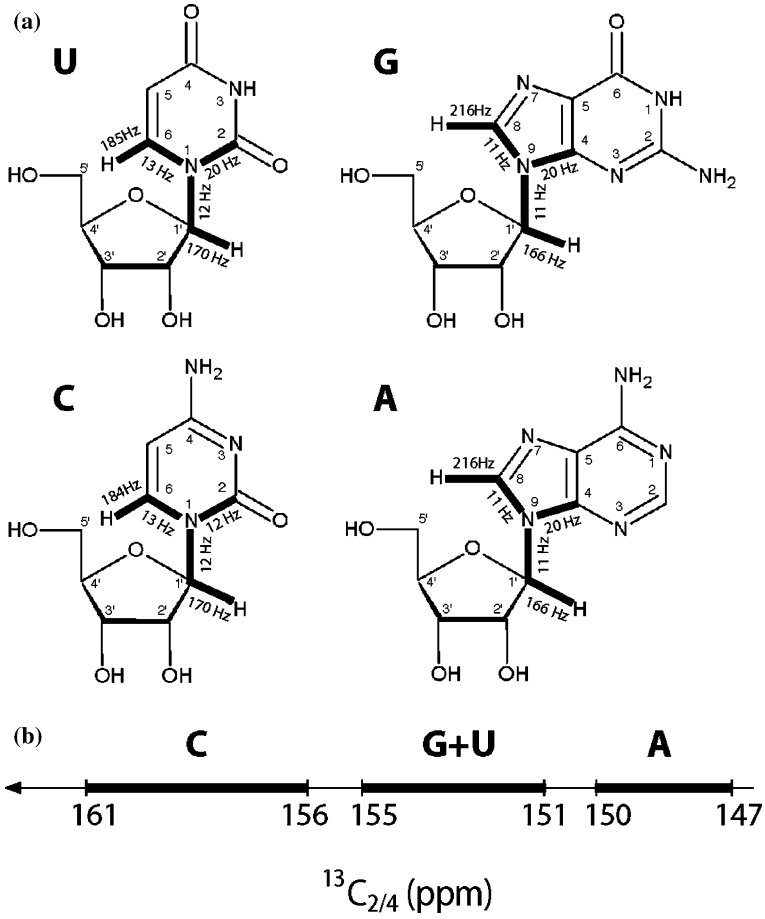

Figure 3. (a) Schematic representation of the 4 RNA nucleosides. Thick lines highlight the nuclei involved in the coherence transfer pathway of the CT-HCN(C) experiment. The coupling constants are given according to Wijmenga and Van Buuren (1998). (b) ^{13}C chemical shift ranges for the quaternary carbons involved in the base-type spectral-editing filter: C_4 for G and A, and C_2 for U and C nucleotides. The frequency bands were defined on the basis of the available chemical shift data for four different RNA, the 33-nucleotide RNA aptamer used in the present study, a 25-nucleotide stem-loop RNA (Fiala et al., 2004), a 14-nucleotide RNA tetraloop (Furtig et al., 2004), and a 16-nucleotide stem loop currently studied in our laboratory.

both experiments, as usual for Hadamard-type spectral editing.

An example of a base-type-edited 2D MQ-TROSY CT-H(C)N(C) correlation spectrum, recorded using the pulse sequence of Figure 1a (with $t_2 = 0$), is shown in Figure 4a and b. The data were acquired at 800 MHz ^1H frequency on a sample of the uniformly ^{13}C, ^{15}N labeled 33-nucleotide RNA aptamer-theophylline complex. The corresponding spectrum recorded with the sequence of Figure 1b is shown in Figure S1 of the Supporting Information. The CT delay has been adjusted experimentally to $T = 57$ ms (including the duration of the $^{13}C^{all}$ and $^{13}C^{sel}$ pulses applied during the CT delay). This corresponds to slightly smaller coupling constants $J_{N9C4}(G) = J_{N1C2}(U) \approx 17.5$ Hz compared to the values (see Figure 3a) given by Wijmenga et al. (1998). This finding is also confirmed by a recent experimental work of Jaroniec et al. (2005). Using this optimized CT delay, the addition and subtraction of the 2 data sets recorded for base-type filtering results in a clean separation of cross peaks from C and A nucleotides (Figure 4a) and from U and G nucleotides (Figure 4b). This is illustrated by 1D traces, extracted at the N_1 frequency of residue C27, shown in the spectra of Figure 4a and b. The high signal to noise ratio in the C/A sub-spectrum, and the absence of any residual peak intensity detected in the U/G sub-spectrum clearly demonstrate the

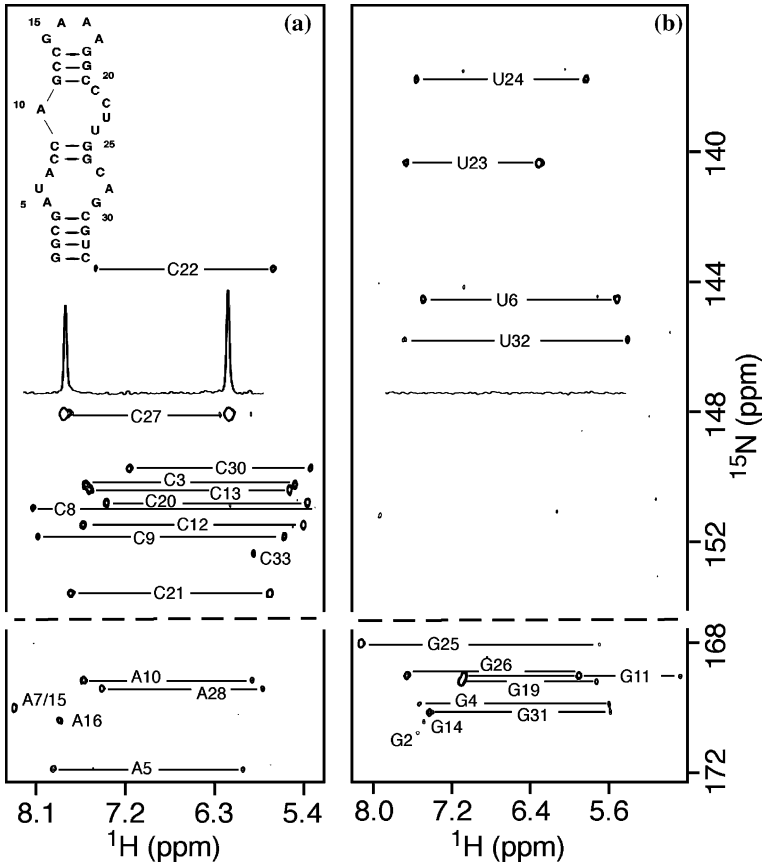

Figure 4. 2D H(C)N correlation spectra recorded using the TROSY CT-HCN(C) pulse sequence of Figure 1a with base-type spectral editing. The data were acquired on a 1.0 mM uniformly ^{13}C,^{15}N-labeled sample of the 1:1.2 33-nucleotide aptamer-theophylline complex at 800 MHz ^{1}H frequency and 25 °C in an overall experimental time of 14hours. The spectrum shown in (a) contains only cross peaks from C and A nucleotides, whereas the spectrum in (b) shows those from U and G. For simplicity the ^{15}N frequency gap between N_9 (purines) and N_1 (pyrimidines) is not shown. Assigned peak pairs are annotated by their base type and residue number. The 1D ^{1}H traces shown in (a) and (b) were extracted at the ^{15}N frequency of C27 illustrating the good filter performance for this nucleotide. In addition, the secondary structure of the RNA aptamer is drawn in the upper left corner in (a).

good filter performance. This base-type filter is particularly useful to improve spectral resolution in the crowded spectral region corresponding to the overlapping A and G cross peaks, as illustrated for the two nucleotides A10 and G26 resonating at the same $N_{1,9}$ frequency. The long acquisition time in the ^{15}N dimension ($t_1^{max} = 50$ ms) that has been further doubled during processing by mirror image linear prediction (Zhu and Bax, 1990) ensures high spectral resolution ($\Delta\nu_{res} \approx 10$ Hz). Both, the enhanced resolution and the base-type discrimination allows unambiguous assignment of all observed peak pairs for this RNA. Note that the missing cross peaks are also absent (or of very low intensity) from a standard TROSY-HCN spectrum most likely due to conformational exchange line broadening. Additional ^{13}C frequency labeling in the 3D version of the experiment provides the required spectral resolution to discriminate between the sugars and bases of different nucleotides. For the 33-nucleotide RNA aptamer studied here, unambiguous intranucleotide base-sugar connectivity assignment ($H_{1'}$-$C_{1'}$-$H_{6,8}$-$C_{6,8}$) was obtained from a 3D MQ-TROSY CT-HCN(C) data set (data not shown). The sensitivity of TROSY or MQ-TROSY CT-HCN(C) is somewhere in between relaxation-optimized HCN and HC(NC)H experiments. It therefore presents a good compromise between sensitivity and spectral resolution for application to larger RNA molecules at high field NMR spectrometers, especially if a cryogenic probe is available that provides the required higher sensitivity.

The base-type edited CT-TROSY HCN experiment also provides a convenient method for base-type identification, which is crucial for sequential RNA resonance assignment. Pulse sequence elements to select or separate NMR signals originating from different types of nucleotides in RNA have been proposed in the past. For example, the H_6-C_6 correlation peaks of pyrimidines can be separated from H_8-C_8 correlation peaks of purines based on the presence or absence of a scalar $^1J_{CC}$ coupling. The distinct chemical shift ranges of the C_5 carbons in U and C bases can be exploited to further separate the H_6-C_6 correlation peaks (Brutscher et al., 2001). Alternatively, experiments designed to correlate different protons within the same base allow selection of a single base type by exploiting a base-type-specific coherence transfer pathway (Simorre et al., 1995; Simorre et al., 1996a; Simorre et al., 1996b). The spectral sediting filter in the CT-HCN(C) experiments proposed here creates two sub-spectra. Signals originating from C and A nucleotides are detected in one sub-spectrum, while signals arising from U and G nucleotides are observed in the second sub-spectrum (Figure 4). For each spectrum, the distinct ^{15}N chemical shift ranges for N_9 (A, G) and N_1 (C, U) allow to further distinguish between purine and pyrimidine cross peaks. Therefore, as long as the C_2 of pyrimidines and C_4 of purines resonate within the frequency bands (Figure 3b) used for the filtering, the base-type edited CT-HCN(C) experiment allows discrimination between all four nucleotides. The performance of the base-type filter is further demonstrated by application to a second RNA. Figure S2 of the Supporting Information shows 2D $^1H-^{15}N$ spectra recorded with the pulse sequence of Figure 1b for a 16-nucleotide ^{15}N,^{13}C labeled stem loop RNA in complex with a 16-nucleotide unlabeled stem-loop RNA. Again a clean separation of cross peaks from the four different nucleotide types is obtained. Therefore, in view of the quite different secondary and tertiary structures of the two RNA molecules, one may expect similar results for other RNA samples. The CT-HCN(C) experiment is to the best of our knowledge the first spectroscopic method providing base-type identification of base ($H_{6/8}$, $C_{6/8}$) and sugar ($H_{1'}$, $C_{1'}$) resonances within a single experiment.

In summary, we have shown that highly resolved HCN correlation spectra can be recorded using new transverse relaxation optimized CT-HCN(C) pulse sequences including a base-type spectral editing filter. The base-type filter not only increases spectral resolution, but it also provides a simple way of base-type identification, an information which otherwise is difficult to obtain. Therefore we expect that this experiment will become a widespread tool for NMR studies of larger RNA molecules. This pulse scheme may prove equally useful for application to DNA provided that the constant time delay T and the frequency band of the inverted quaternary ^{13}C are properly adjusted.

Supporting information available

One figure showing 2D $^1H-^{15}N$ correlation spectra of the 33-nucleotide aptamer-theophylline complex recorded with the MQ version of the CT-HCN(C) pulse sequence of Figure 1b with base-type spectral editing. One figure showing the 2D base-type edited $^1H-^{15}N$ correlation spectra of a 16 nucleotide ^{13}C,^{15}N-labeled RNA in complex with a 16 nucleotide unlabeled RNA. This material is available in electronic form at http://dx.doi.org/10.1007/s10858-005-8872-1.

Acknowledgements

We thank Ad Bax for the sample of a complex formed by two RNA stem loops, and Marella Canny for sample preparation of the 33-nucleotide aptamer. This work was supported by the Commissariat à l'Energie Atomique, the Centre National de la Recherche Scientifique, and NIH (AI33098). H.V.M. acknowledges the receipt of a fellowship from the C.E.A. J.B. acknowledges support from the HFSP Organization.

References

Brutscher, B., Boisbouvier, J., Kupce, E., Tisne, C., Dardel, F., Marion, D. and Simorre, J.P. (2001) *J. Biomol. NMR*, **19**, 141–151.

Brutscher, B., Boisbouvier, J., Pardi, A., Marion, D. and Simorre, J.P. (1998) *J. Am. Chem. Soc.*, **120**, 11845–11851.

Brutscher, B. and Simorre, J.P. (2001) *J. Biomol. NMR*, **21**, 367–372.

Duchardt, E., Richter, C., Ohlenschlager, O., Gorlach, M., Wohnert, J. and Schwalbe, H. (2004) *J. Am. Chem. Soc.*, **26**, 1962–1970.

Farmer, B.T., Muller, L., Nikonowicz, E.P. and Pardi, A. (1994) *J. Biomol. NMR*, **4**, 129–133.
Farmer, B.T., Müller, L., Nikonowitz, E.P. and Pardi, A. (1993) *J. Am. Chem. Soc.*, **115**, 11040–11041.
Fiala, R., Czernek, J. and Sklenar, V. (2000) *J. Biomol. NMR*, **16**, 291–302.
Fiala, R., Jiang, F. and Sklenar, V. (1998) *J. Biomol. NMR*, **12**, 373–383.
Fiala, R., Munzarova, M.L. and Sklenar, V. (2004) *J. Biomol. NMR*, **29**, 477–490.
Furtig, B., Richter, C., Bermel, W. and Schwalbe, H. (2004) *J. Biomol. NMR*, **28**, 69–79.
Furtig, B., Richter, C., Wohnert, J. and Schwalbe, H. (2003) *Chembiochem.*, **4**, 936–962.
Geen, H. and Freeman, R. (1991) *J. Magn. Reson.*, **93**, 93–141.
Hadamard, J. (1893) *Bull. Sci. Math.*, **17**, 240–248.
Hu, W.D., Gosser, Y.Q., Xu, W.J. and Patel, D.J. (2001) *J. Biomol. NMR*, **20**, 167–172.
Jaroniec, C.P., Boisbouvier, J., Tworowska, I., Nikonowicz, E.P. and Bax, A. (2005) *J. Biomol. NMR*, **31**, 231–241.
Kupce, E., Boyd, J. and Campbell, I.D. (1995) *J. Magn. Reson.*, **106**, 300–303.
Kupce, E. and Freeman, R. (1993) *J. Magn. Reson.*, **105A**, 234–238.
Kupce, E. and Freeman, R. (1996) *J. Magn. Reson.*, **118A**, 299–303.
Kupce, E. and Freeman, R. (2003) *J. Magn. Reson.*, **162**, 158–165.
Marino, J.P., Diener, J.L., Moore, P.B. and Griesinger, C. (1997) *J. Am. Chem. Soc.*, **119**, 7361–7366.
Pervushin, K., Riek, R., Wider, G., and Wüthrich, K. (1997) *Proc. Natl. Acad. Sci. USA*, **94**, 12366–12371.
Ravindranathan, S., Kim, C.H. and Bodenhausen, G. (2003) *J. Biomol. NMR*, **27**, 365–375.
Riek, R., Pervushin, K., Fernandez, C., Kainosho, M. and Wuthrich, K. (2001) *J. Am. Chem. Soc.*, **123**, 658–664.
Shaka, A.J. and Pines, A. (1987) *J. Magn. Reson.*, **71**, 495–503.
Simorre, J.P., Zimmermann, G.R., Mueller, L. and Pardi, A. (1996a) *J. Biomol. NMR*, **7**, 153–156.
Simorre, J.P., Zimmermann, G.R., Mueller, L. and Pardi, A. (1996b) *J. Am. Chem. Soc.*, **118**, 5316–5317.
Simorre, J.P., Zimmermann, G.R., Pardi, A., Farmer, B.T. and Mueller, L. (1995) *J. Biomol. NMR*, **6**, 427–432.
Sklenar, V., Peterson, R., Rejante, M. and Feigon, J. (1993a) *J. Biomol NMR*, **3**, 721–727.
Sklenar, V., Peterson, R.D., Rejante, M.R., Wang, E. and Feigon, J. (1993b) *J. Am. Chem. Soc.*, **115**, 12181–12182.
Tate, S., Ono, A. and Kainosho, M. (1994) *J. Am. Chem. Soc.*, **116**, 5977–5978.
Van Melckebeke, H., Simorre, J.P. and Brutscher, B. (2004) *J. Am. Chem. Soc.*, **126**, 9584–9591.
Wijmenga, S.S. and Buuren, B.N.M.van (1998) *Prog. in Nucl. Magn. Reson. Spectroc.*, **32**, 287–387.
Yan, J.L., Corpora, T., Pradhan, P. and Bushweller, J.H. (2002) *J. Biomol. NMR*, **22**, 9–20.
Zhu, G. and Bax, A. (1990) *J. Magn. Reson.*, **90**, 405–410.
Zimmermann, G.R., Jenison, R.D., Wick, C.L., Simorre, J.P. and Pardi, A. (1997) *Nat. Struct. Biol.*, **4**, 644–649.